Separation and Purification Technology 179 (2017) 248–256

Contents lists available at ScienceDirect

Separation and Purification Technology

journal homepage: www.elsevier.com/locate/seppur

Utilization of acetic acid-[(hydrazinylthioxomethyl)thio]-sodium as a novel selective depressant for chalcopyrite in the flotation separation of molybdenite

Zhigang Yin, Wei Sun *, Yuehua Hu, Chenhu Zhang, Qingjun Guan, Runqing Liu *, Pan Chen, MengJie Tian

School of Minerals Processing and Bioengineering, Central South University, Changsha, Hunan 410083, China

ARTICLE INFO

Article history:
Received 27 October 2016
Received in revised form 9 January 2017
Accepted 21 January 2017
Available online 9 February 2017

Keywords:
Chalcopyrite
Molybdenite
Depressant
AHS
Separation

ABSTRACT

The flotation response of chalcopyrite and molybdenite when using a novel compound, acetic acid-[(hydrazinylthioxomethyl)thio]-sodium (AHS), as the depressant was investigated through micro-flotation and batch flotation in this study. The depressing mechanisms were studied by means of zeta potential, FTIR and XPS measurements. The micro and bench flotation results indicated that AHS exhibited a strong influence on the depression of chalcopyrite and had little effect on the flotation of molybdenite minerals; these results might be attributed to the significant improvement of the molybdenite/chalcopyrite selectivity index after the addition of AHS. The results of the FTIR spectra, zeta potential and XPS measurements indicated that AHS chemisorbs onto the chalcopyrite surface through its S and N atoms, forming a five-membered cheat ring. A possible depressant mechanism along with a postulated adsorption mode for the surface interaction between AHS and chalcopyrite are provided.

1. Introduction

In the mineral processing industry, selective separation of valuable minerals from gangues is commonly achieved by froth flotation. Selective separation of minerals by froth flotation usually relies on the use of various chemical reagents (e.g., collector, frother and depressant) that affect the floatability of individual ore components [1]. In the case of the naturally floatable minerals molybdenite and chalcopyrite, the selective depressants that are used usually depend on the selected process for conducting the separation. Selective separation of copper or lead-molybdenum sulphide minerals by flotation could be realized by adopting different depressant systems [2]. If molybdenite is the primary economic mineral, then depressants are usually added to depress the unwanted sulphide mineral in the ore, such as chalcopyrite, galena, and pyrite. The reported depressants for depressing these sulphide ore include sodium hydrosulphide [3], DPS [4], sodium sulphide [5,6], cyanide [7], PGA [8], 2,3-disulfanylbutanedioic acid (DMSA) [9], thioglycollic [10], Noke's reagent and the combination of organic and inorganic depressants [11,12]. However, when molybdenite occurs with polymetallic sulphide minerals (such as chalcopyrite and galena), direct separation of molybdenite from the associated ore is not economical. In these cases, the molybdenum bulk concentrate was obtained with the other sulphides and can subsequently be selectively floated or depressed [13]. The reagents used for depressing molybdenite are usually hydrophilic polymers, such as polyacrylamide, humic acids, lignosulphonates, dextrin, starch, glue and dyes [13–15]. The strategy of floating molybdenite rather than chalcopyrite/galena is largely dictated by the mass balance of different metals. The content of chalcopyrite or galena in chalcopyrite or galena-molybdenite bulk concentrate is usually much higher compared to the content of molybdenite; as a result, the depression of molybdenite and simultaneous flotation of chalcopyrite or galena would inevitably lead to poor separation results because of the mechanical entrainment of molybdenite within chalcopyrite or galena concentrate [14]. As mentioned above, the common flotation practice of separating molybdenite from chalcopyrite or other sulphide ores usually relies on the flotation of molybdenite while depressing the other unwanted sulphide ores. Although considerable work has been performed on the use of different depressants for the selective separation of molybdenite from a polymetallic ores, the drawbacks of the reported depressants cannot be ignored: (a) the toxic nature of most of these depressants; (b) the high dosage and low selectivity of some of the depressants; and (c) the difficulty of replacing these high dosage, low selectivity and toxic or hazardous reagents with more environmentally friendly and economical chemicals under industrial conditions. Therefore, the development of new depressants that have a

* Corresponding authors.
E-mail addresses: sunmenghu@csu.edu.cn (W. Sun), liurunqing@126.com (R. Liu).

http://dx.doi.org/10.1016/j.seppur.2017.01.049
1383-5866/

low cost, good stability and non-toxic or low-toxic compounds for Cu-Mo separation is still a challenging task that will attract much attention in the future.

Dithiocarbazic and its substituted derivatives have received considerable attention over the past few decades [16]. Interest remains high in these compounds and Schiff bases because of the following reasons: (a) dithiocarbazic acid and the Schiff bases derived from them through condensation with various aldehydes and ketones because of the specific geometries of metal complexes [17] and (b) the wide variation in their structures and properties, especially because of their bioactivity [18]. The presence of nitrogen and sulphur atoms in the molecular structure of dithiocarbazates provides them with a good ability to coordinate metal ions and form five-membered chelate rings, yielding metal complexes with interesting structural and properties [19]. The metal complexes (such as Cu(II), Ni(II), Co(II), Zn(II), Cr(III), Pd(II), Fe(III) and Sb (III)) of dithiocarbazate derivatives have been widely studied because of their potential for therapeutic use [20,21], effective single-source precursor [22], catalysis [23], photocatalytic production of hydrogen [24], non-linear optical properties [25], and biological properties [18].

Publications to date have mainly focused on the synthesis, characterization and bioactivity of dithiocarbazate and its derivatives because of their promising applications in the fields mentioned above. However, to our knowledge, there is no literature report on the application of dithiocarbazate and its derivatives in the field of mineral processing, let alone on the separation of copper and molybdenum by flotation. It is expected that dithiocarbazate and its derivatives could potentially form metal complexes on mineral surfaces and make the surface hydrophilic, thus depressing the flotation of specific minerals in the flotation separation process. Motivated by the powerful ability of dithiocarbazate and its derivatives to coordinate with metal ions and form chelate rings, it was considered worthwhile to develop a new dithiocarbazic acid derivative that can be applied to the field of differential flotation separation of copper-molybdenum minerals. Thus, in the present investigation, acetic acid-[(hydrazinylthioxomethyl)thio]-sodium (AHS) was designed, synthesized and adopted as a potential depressant in copper-molybdenum sulphide separation using pure minerals and the bulk copper-molybdenum concentrate collected from Yichun Luming Mining Co., Ltd, China, to determine its potential for use as an effective selective depressant. Zeta potential, FTIR spectroscopic and XPS measurements were conducted to illustrate the interaction mechanisms between AHS and chalcopyrite.

2. Experimental

2.1. Sample and reagents

2.1.1. Samples

Molybdenite and chalcopyrite were obtained from China Molybdenum Co., Ltd., and Dexing copper Mine, respectively. The minerals were crushed in a porcelain mortar and then sieved. The size of the sample particles in the range of 38–74 μm was used for flotation. Each sample was treated with dilute nitric acid (0.1 M) to eliminate oxide layers and dilute sodium hydroxide (0.1 M) to remove any hydrophobic impurities. After each leaching step, the residues were removed by washing the sample with distilled water until neutral. The sample was dried in vacuum desiccators, kept in a plastic bag, and then stored in a freezer to minimize oxidation. The XRD spectra (Fig. 1 (supplementary material) and XRF analysis results (not shown) confirmed that the chalcopyrite and molybdenite samples were both had a purity of over 90%.

The bulk concentrate, which was obtained from the Yichun Luming Mining Co., Ltd. with 0.28% Cu and 1.05% Mo collected from a day shift, was used for the flotation separation of copper molybdenum sulphides in the batch flotation tests. The mineralogical data confirmed that both copper and molybdenum mainly existed in the form of chalcopyrite and molybdenite, respectively. Meanwhile, the XRD data confirmed that the predominate gangue minerals were pyrite, galena, sphalerite, quartz and mica. The size distribution of the feed material (bulk concentrate) was determined using a Mastersizer 2000 (Malvern Instruments Ltd, UK). A typical size distribution of the feed material is given in Fig. 1d (supplementary material). It can be seen from Fig. 1 (supplementary material) that the F80 and F50 of the bulk concentrate are approximately 60 μm and 20 μm, respectively.

2.1.2. Reagents

The following chemicals were of analytical grade, purchased from local suppliers and used without further purification: sodium chloroacetate (Guangfu Chemical Co., Ltd.), hydrazine hydrate (Xilong Chemical Co., Ltd.), carbon disulphide (Kelong Chemical Co., Ltd.), sodium hydroxide and ethanol (Sinopharm Chemical Reagent Co., Ltd.), and copper sulphate pentahydrate (Aladdin Chemical Reagent Co., Ltd.). Distilled water was used for microflotation, zeta-potential and sample preparation for FTIR spectroscopic and XPS measurements.

The depressant acetic acid-[(hydrazinylthioxomethyl)thio]-sodium was synthesized according to the known methods of Ali and Bera [16,24]; the synthetic route is shown in Fig. 2 (supplementary material). Briefly, 4 g of sodium hydroxide (0.1 mol) was dissolved in 30 ml of absolute ethanol with 5 g of hydrazine hydrate (0.1 mol) added, and then, the mixture was cooled to 0 °C in an ice-salt bath. Carbon disulphide (7.6 g, 0.1 mol) was added dropwise with constant stirring over a period of 4 h. A yellow product was obtained after the complete addition of carbon disulphide, and then, the reaction mixture was stirred for another half an hour. The yellow product was separated and dissolved in 40% aqueous cold ethanol (30 mL). The mixture was again kept in an ice-salt bath and 11.7 g of sodium chloroacetate (0.1 mol) dissolved in 30 mL of distilled water was added dropwise while maintaining the temperature between 0 and 5 °C. After the complete addition of the sodium chloroacetate solution, the solution was condensed by a rotary evaporator at 80 °C and then cooled in an ice-salt bath; the resulting white product formed was filtered off and finally washed with 40% aqueous ethanol. Recrystallisation from water-ethanol solution yielded a pure white powder product.

2.2. Methods

2.2.1. Chemical analysis

Spectrophotometric analysis of samples was conducted using standard methods for Mo analysis (T6 UV visible single beam spectrophotometer, Beijing Purkinje General Instrument Co., LTD, China). Copper was determined using inductive couple plasma spectrometry (Thermo Fisher ICE-3500, USA).

2.2.2. Micro-flotation tests

A flotation machine of the XFG-1600 type (mechanical agitation) with a volume of 40 mL, which was manufactured by Jilin prospecting machinery factory (China), was used in microflotation tests. The impeller speed was fixed at 1902 rpm. The mineral suspension was prepared by adding 2.0 g of a single mineral to 40 mL of solutions in single mineral flotation tests. The mineral surfaces were cleaned by using an ultrasound cleaner, and the pH of the mineral suspension was adjusted to the desired operating value by adding HCl or NaOH stock solutions. The depresant (AHS 20 mg/L), collector (Kerosene 200 mg/L) and frother (MIBC)

were respectively added into the flotation cell with 2 min conditioning time. Flotation concentrates were then collected for a total of 5 min. The floated and unfloated particles were collected, filtered and dried. In a single mineral flotation, the recovery was calculated based on the solid weight distributions between the two products. To assess the accuracy of flotation tests, the errors of the recovery were found to be within 2.0% after at least three tests under each condition, and the average values were reported.

2.2.3. Bench-scale flotation tests

The experimental runs were conducted in an XFD type flotation cell with a volume capacity of 1.5 L, which was manufactured by Jilin prospecting machinery factory (China). The feed was added to the flotation cell with tap water to obtain the required pulp density. The pulp density (solid %) was adjusted to be 50% at conditioning and 33% during flotation. Next, the required amount of depressant was added and conditioned for four minutes. The flotation time was 5 min, according to the results of the previous experiment (not shown). The flow sheet and conditions of the flotation tests are shown in Fig. 3 (supplementary material). Both the concentrate and tailings were filtered, dried, weighed and analysed.

2.2.4. Zeta potential measurements

Zeta potential experiments were conducted using the Malvern Zeta Sizer Nano Series (manufactured in England). Zeta potential measurements for each mineral were performed in a 0.01 M NaCl electrolyte solution. A suspension containing 0.01 wt% of freshly ground mineral particles (100% passing 5 μm) was prepared in the electrolyte solution. The measurements were conducted at room temperature (±1 °C). The pH of the mineral suspension was adjusted to the desired operating value by adding HCl or NaOH stock solutions. In addition, measurements were also performed with the addition of a depressant at a constant concentration (100 mg/dm^3). The results presented were the average of three independent measurements, with a typical variation of ±2 mV.

2.2.5. FTIR spectrum

The infrared spectra of samples embedded in KBr pellets were recorded by a Bruker Alpha (Thermo, USA) FT-IR spectrometer at room temperature (25 ± 1 °C) in the range from 400 cm^{-1} to 4000 cm^{-1}. At 25 °C, 100 mg of mineral samples were added to 50 mL of an aqueous solution with or without 100 mg/L depressant at pH 8. After stirring for half an hour, the mineral samples were filtered, washed three times with distilled water and then dried in a vacuum oven at room temperature for 24 h.

2.2.6. XPS analysis

The XPS spectra of mineral particles before and after depressant adsorption were recorded with a K-Alpha 1063 (Thermo Scientific Co., USA) spectrometer with an Al Kα sputtering-ray source operated at 12 kV and 6 mA and a pressure in the analytical chamber of 1.0×10^{-12} Pa. All of the binding energies were referenced to the neutral C1s peak at 284.8 eV to compensate for the surface-charging effects. XPS Peak 4.1 software was used to fit the XPS peaks.

3. Results and discussion

3.1. Micro-flotation tests

3.1.1. Effect of the pH value

Fig. 4 (supplementary material) presents the flotation results of chalcopyrite and molybdenite as a function of pH (4–12) in the presence and absence of AHS. The recoveries of both chalcopyrite and molybdenite are found to decrease slightly with increasing pH over the tested pH range. As shown in Fig. 4 (supplementary material), both molybdenite and chalcopyrite show high floatability, with a high recovery of more than 90% and 80%, respectively, in the pH range in the absence of AHS. The floatability of chalcopyrite is similar to that of molybdenite in the tested pH range, which indicates that it is difficult to separate chalcopyrite and molybdenite in the absence of a depressant. The high recovery of chalcopyrite might attributed to the formation of sulphur elements, as discussed in the following section (XPS analysis), which is in agreement with the reports [2].

However, when 20 mg/L AHS was added, the recovery of chalcopyrite decreased from 83% to approximately 25% at pH 8. With the increase of pH, the recovery of chalcopyrite slightly decreased and remained at approximately 15% at pH 12. In comparison, the recovery of molybdenite decreased slightly when AHS was introduced in the tested pH range. It can be concluded that AHS had a slight depression effect on molybdenite, whereas the recovery of chalcopyrite decreased dramatically. It is clear that the maximum recovery difference between chalcopyrite and molybdenite occurred over the pH range of 8–10. Therefore, the pH value of 8 was chosen to perform the following conditional experiments, which are close to neutral and economical in Cu-Mo commercial flotation separation.

3.1.2. Effect of AHS dosage

The effect of the AHS dosage on the flotation recovery of chalcopyrite and molybdenite at pH 8 is shown in Fig. 5 (supplementary material). The floatability of chalcopyrite decreased significantly, whereas the recovery of molybdenite decreased slowly with increasing depressant dosage, indicating that AHS had little effect on the floatability of molybdenite. Moreover, the result also showed that the recovery difference between molybdenite and chalcopyrite gradually increased as the depressant concentration increased; however, when the dosage reached 40 mg/L, increasing the dosage of depressants had no obvious effect on the separation of chalcopyrite from molybdenite. Under this condition, a separation window with 82.2% separability was obtained using AHS at a concentration of 40 mg/L. Therefore, it is possible to use AHS as a potential selective depressant in copper-molybdenum separation by flotation.

3.2. Bench-scale flotation tests

3.2.1. Effect of the depressant on chalcopyrite flotation

The selective separation of chalcopyrite and molybdenite is one of the difficult problems in polymetallic sulphide ore processing. To perform selective separations of the two minerals by flotation, depressants play an important role. As stated in the pure mineral flotation tests section, AHS has been shown to exhibit a strong depressing effect on chalcopyrite. However, the pure mineral flotation tests could not demonstrate the competitive adsorption of AHS on the two minerals. Therefore, further tests were conducted on copper-molybdenum bulk concentrate to evaluate the potential for using AHS as a selective depressant in copper-molybdenum separation (Fig. 3). The effect of the depressant was estimated by varying the dosage from 0 to 60 g/t. The results of the flotation studies as a function of the AHS concentration is shown in Fig. 6 (supplementary material). As seen in Fig. 6 (supplementary material), as the depressant concentration increased, only a small effect on Mo recovery was observed. At the same time, the recovery of Cu gradually decreased with the increase of the depressant concentration; however, the recovery decreased slowly when the depressant was increased to a certain concentration. At a concentration of 40 g/t, the recovery of Mo and Cu was 91.55% and 16.82%.

As well knonw that a certain amount of AHS in the flotation system helps to depress the chalcopyrite particles, resulting in a better

selectivity of the reagent towards molybdenite. The flotation separation results of the Cu-Mo bulk concentrate showed that AHS could be used as a selective depressant in copper-molybdenum separation with the advantages of a lower dosage and environmentally friendly nature compared to a conventional depressant, such as sodium sulphide, Nokes reagents, and cyanide.

3.2.2. Kinetic flotation tests with and without AHS

The effects of the depressant on the kinetic flotation performance with and without AHS were investigated according to the beneficiation flowsheet presented in Fig. 3 (supplementary material). Among the many flotation models, the classical first-order flotation model is the most widely accepted and is used here to demonstrate the calculation of the proposed modified rate constant and selectivity index [26].

$$R = R_{\infty}\left[1 - \exp^{(-kt)}\right] \quad (1)$$

$$K_M = R_{\infty} \cdot k \quad (2)$$

$$S.I.(I/II) = (K_M \text{ of mineral I})/(K_M \text{ of mineral II}) \quad (3)$$

where R is the recovery of minerals at time t, R_{∞} is the ultimate recovery, k is the first-order rate constant, K_M is the modified rate constant, and S.I.(I/II) is the selectivity index of mineral I over mineral II in the same flotation system. Fig. 7 (supplementary material) shows the recovery of molybdenite and chalcopyrite as a function of the flotation time along with the corresponding model fits (with and without AHS). The lower flotation rate responds to fine mineral particles. This behaviour is mainly attributed to the small mass of the particles, leading to a lower probability of collision and adhesion of particles to an air bubble; this result is in good agreement with the size distribution of the feed material (Section 2.1.1) and could be improved by floc-flotation [27]. The model parameters K, K_M, R_{∞} and S.I. (selectivity index) are shown in Table. 1. For molybdenite, using AHS as the depressant decreased the ultimate recovery from 78.80% to 76.98%, whereas the constant k increased from 0.96 to 0.97. For chalcopyrite, the addition of a depressant decreased both R_{∞} and k. The results indicated that the Mo recovery was affected by the higher concentration of the depressant (the depressants used for bench flotation were prepared according to the reports in Section 2.1.2 without purification); this effect may be explained by the fact that strongly alkaline solutions have a negative effect on molybdenite flotation [28].

In terms of the modified rate constant, the introduction of a depressant decreased the value of km for chalcopyrite, but the value of km for molybdenate did not change. It is clear that the molybdenite/chalcopyrite selectivity index in the presence of AHS is far better (four fold) than in the absence of AHS, indicating that AHS has a good selective depressing effect for chalcopyrite. The difference in the selectivity index greatly contributes to the polar group structure of AHS, which could react with both transition and main group metals through its S and N atoms.

3.3. Zeta potential measurement

In this section, the zeta potentials of chalcopyrite before and after treatment with AHS were studied. The changes of the charge on the surface of chalcopyrite were related to the adsorption of reagents; these changes help to illustrate the interaction mechanism between the depressant and mineral surface [29]. The zeta potential of chalcopyrite as a function of pH with and without AHS is shown in Fig. 8. The figure indicates that the isoelectric point (IEP) of chalcopyrite was found to be approximately pH 5.00, which was in accordance with those previously reported [30,31]. After interaction with AHS, the zeta-potential of chalcopyrite shifted towards a more negative value in the tested pH range, demonstrating that AHS had a strong effect on the zeta-potential of chalcopyrite and the adsorption of AHS on the chalcopyrite surface was increased significantly.

AHS is an anionic compound, the main species of which exist as its anionic species ($(NH_2—NH—C(=S)—S—CH_2—COO)^-$) under alkaline conditions. The strongest depression of chalcopyrite, as measured by flotation, appears to coincide with the strongest decrease in zeta potential at pH 6–12. AHS with two polar groups, such as ($NH_2—NH—C(=S)—$/$NH_2—N=C(—SH)—$) and $—COO^-$, might adsorb on the surface of chalcopyrite, thus reducing the floatability of chalcopyrite. It is well known that ($NH_2—NH—C(=S)—$/$NH_2—N=C(—SH)—$) reacts with chalcopyrite (copper ions) and adsorbs on the mineral surface, in good agreement with the FTIR results (Section 3.4). By contrast, $—COO^-$ is a hydrophilic group that can exchange adsorption with minerals and form a water molecule membrane between the mineral and depressant to increase the hydrophilicity of the mineral surface (which is similar to that of sodium thioglycollate and DMTC), thus promoting a large increase in its electronegativity [11,32].

3.4. FT-IR analysis

The FTIR spectra of AHS and its Cu^{2+} complexes as well as chalcopyrite before and after AHS treatment are presented in Fig. 9. AHS has a thione group with an adjacent imide proton [—NH—C(=S)—] that can exhibit tautomerism to the thiol form [33]. The IR spectra of AHS indicated that the peaks at approximately 3437 cm^{-1} were attributed to the asymmetric and symmetric stretching modes of the NH_2 group, and the absence of a band in the region of 2650–2500 cm^{-1} indicate the absences of a free —SH group. Therefore, in a solid state, AHS is in the thione tautomeric form [34]. The peaks at approximately 1579 and 1417 cm^{-1} were assigned to the mixed vibration of $\upsilon_{(C-N)}$ and $\upsilon_{(N-N)}$, and the peaks that appeared at approximately 1386 cm^{-1} are due to the $\upsilon_{(C-N-N)}$ vibration. The other peaks at 1251, 1056, 934 and 901 cm^{-1} were attributed to the $\upsilon_{(C-H)}$, $\upsilon_{(C=S)}$, [$\upsilon_{(C=S)}$+-$\upsilon_{(C-S)}$] and $\upsilon_{(C-S)}$ of the compound [19], respectively. Fig. 9 shows that after the reaction with Cu^{2+} ions, the C=S peak in AHS at approximately 1056 cm^{-1} almost disappeared in the Cu^{2+}-AHS complexes and the $\upsilon(NH/NH_2)$ peaks at approximately 3442 cm^{-1} were far weaker than those in AHS. Furthermore, the peak of the mixed vibration of $\upsilon_{(C-N)}$ and $\upsilon_{(N-N)}$ as well as the peak of $\upsilon_{(C-N-N)}$

Table 1
Model parameters of the model fits.

Parameters	Without AHS		With AHS	
	Molybdenite	Chalcopyrite	Molybdenite	Chalcopyrite
R_{∞}	78.80	77.84	76.98	19.49
K	0.96	0.67	0.97	0.65
K_M	0.75	0.52	0.75	0.13
S.I. (Mo/Cu)	1.44		5.77	

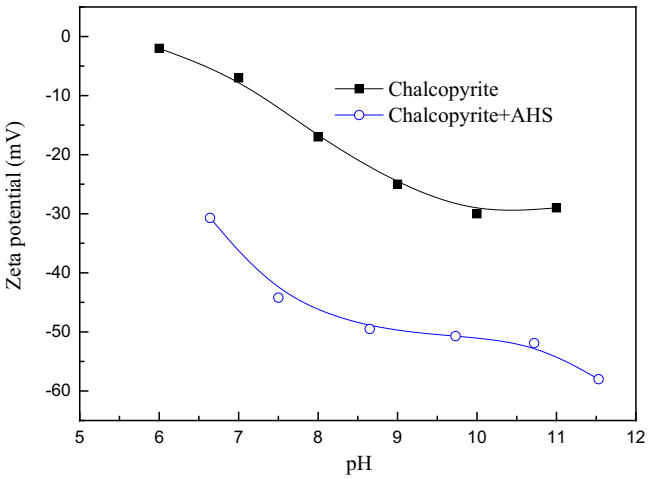

Fig. 8. The zeta potential of chalcopyrite as a function of pH in the absence and presence of AHS (50 mg/L).

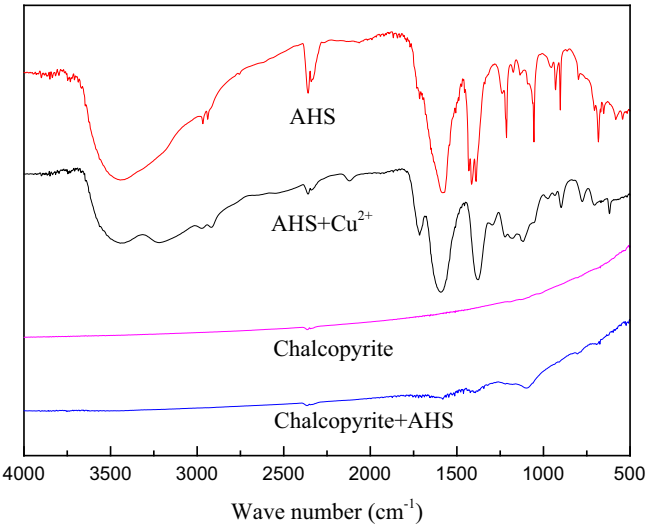

Fig. 9. The FTIR spectra of AHS, AHS-Cu^{2+}, chalcopyrite before and after treatment.

of the AHS-Cu^{2+} reaction product appeared at 1589 and 1379 cm^{-1}, respectively, indicating the involvement of the nitrogen atom of the NH_2 group in bonding. These changes suggest that when AHS reacted with Cu^{2+} in aqueous solutions, its functional group NH_2—NH—C(=S)—S—R rearranged to NH_2—N=C(—SH)—S—R and then the Cu atoms bonded with S and N atoms to form five-membered chelate rings, while the S—H bonds were broken and released H ions into the aqueous solutions [24].

After AHS treatment (Fig. 9), the peaks of the mixed vibration of $\upsilon_{(C-N)}$ and $\upsilon_{(N-N)}$ and the peaks of $\upsilon_{(C-N-N)}$ appeared on the chalcopyrite surfaces. Meanwhile, compared to the C=S peak of AHS at approximately 1056 cm^{-1}, the C=S peak was shifted to the higher energy side by approximately 39 cm^{-1} in comparison with AHS, indicating the participation of the sulphur atom of the C=S group as a possible coordination site. Moreover, the new peaks at approximately 1578 and 1386 cm^{-1} were assigned to the mixed vibration of $\upsilon_{(C-N)}$ & $\upsilon_{(N-N)}$ and $\upsilon_{(C-N-N)}$, respectively, whereas the new bands were similar to the bands of AHS-Cu^{2+} that were present on the chalcopyrite surface due to the probable involvement of the nitrogen atom of the primary amine ($—NH_2$) group in bonding. Bidentate-chelate, acting through one S and one N donor atom and the presence of hard N and soft S donor atoms, enables AHS to react with both transition and main group metals. As a result, AHS can chemisorb onto the chalcopyrite surface through its S and N atoms, thereby forming cheat rings.

3.5. XPS analysis

Fig. 10 shows the survey scan spectra of AHS and of chalcopyrite with and without depressant treatment over a binding energy range of 1200–0 eV. Clearly, the spectrum of the depressant showed that the component elements of AHS, such as C, O, N, S and Na, were detected, and no evidence of contamination or impurities by other elements could be found. The atomic contents of the C, O N, S and Cu atoms are listed in Table 2. The results shown in Table 2 indicate that the atomic concentrations of the C and N atoms in chalcopyrite surfaces increased after AHS treatment, while those of the O, S and Cu atoms decreased, confirming the adsorption of HAS on the chalcopyrite surface.

The high resolution sulphur 2p spectra of AHS, AHS-Cu complex as well as chalcopyrite treated and untreated with depressant were collected, as displayed in Fig. 11. Fig. 11 displays the features of original chalcopyrite, with the strong S 2p peak at 161.41 eV originating from bulk monosulphide, disulphide species (S_2^{2-}) at 162.59 eV and S_n^{2-}/S^0 at 164.02 eV; these features are similar to those of previous reports [35–37]. The fitted S 2p peak at 169.25 eV is attributed to sulphate (SO_4^{2-}), which indicates that the chalcopyrite surface was oxidized [35]. The S 2p spectrum of AHS could be fitted with two components: one at 163.56 eV (—S—) and the other at 164.74 eV (—NH—C(=S)—). After AHS adsorption, the S 2p line can be fitted by four doublets with the position of the S 2p splitting peaks at 161.41 eV, 162.59 eV, 163.82 eV and approximately 164.87 eV. The former two doublets have positions characteristic of the sample of original chalcopyrite [36,38], while the S 2p peaks at 163.82 eV and 164.87 eV could be assigned to S atoms in adsorbed AHS molecules and are shifted upward by 0.26 and 0.13 eV compared with the BE of AHS, respectively. The S 2p spectra of AHS-Cu complex located at 163.78 and 164.96 eV, respectively. Compared with the S 2p spectra of treated chalcopyrite, the S 2p binding energy of AHS-Cu complex shifted to minimum higher binding energy indicating that the reaction between AHS chalcopyrite might the same as the reaction of copper complex. In other words, the AHS might chemisorbed on chalcopyrite surface by formation of copper complex. The sulphate species vanished with the addition of depressant, further indicat-

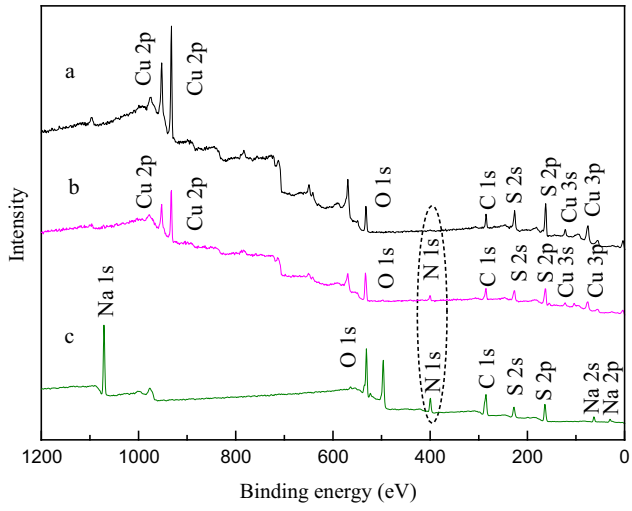

Fig. 10. The survey (full range) XPS spectra of AHS, chalcopyrite before and after treatment ((a) before treatment, (b) after treatment and (c) AHS).

Table 2
Element atomic contents of samples before and after treatment.

Samples	Atomic concentration of elements (atomic %)				
	C	O	N	S	Cu
Before treatment	34.82	33.65	0.00	19.35	12.17
After treatment	40.09	23.25	9.51	15.36	11.78
Δ^a	5.27	-10.4	9.51	-3.99	-0.39

Δ^a is defined as the value after depressant treatment minus that before treatment.

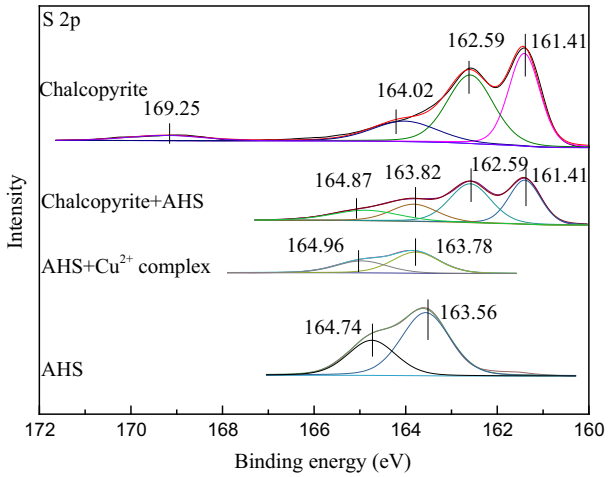

Fig. 11. S 2p spectra of AHS, AHS-Cu^{2+}, chalcopyrite before and after treatment.

ing that the oxidation of chalcopyrite is hindered after the addition of AHS, that is, a layer of AHS molecules might be adsorbed on the chalcopyrite surface.

The C 1s spectra of the AHS + Cu^{2+} complexes, chalcopyrite before and after AHS treatment are summarized in Fig. 12. The C 1s spectrum of the original chalcopyrite has only one peak at 284.82 eV. After interacting with Cu^{2+} ions, the C 1s spectrum could be fitted with four components. The major peak at 284.2 eV is assigned to the referenced C 1s, and the other three components at 286.15, 286.87 and 288.72 eV can be assigned to methylene (—CH_2—); C bound to S (single bond), S (double bond) and N (single bond)(—NH—C(=S)—S); and C bound to O (C=O) in the AHS molecule. These binding energy findings, that is increased binding energy, were very close to the reported C 1s of IPETC (ethyl C bounded to N, 286.1 eV) [39], CS_2 and ethyl xanthate (286.5 eV) [40], and carbon in BECTU (C=O, 288.8 eV) [41]. After conditioning in AHS solution, the C 1s spectra of chalcopyrite can be fitted into four components. Apart from the reference peak at 284.81 eV, the remaining peaks at 285.83, 286.58 and 288.37 eV were attributed to the corresponding C 1s peaks mentioned above, providing further evidence of the adsorption of AHS on the chalcopyrite surface.

The N 1s spectra of AHS, AHS-Cu^{2+} complexes, chalcopyrite before and after AHS treatment are shown in Fig. 13. The N 1s spectrum of AHS can be fitted by two doublets with the positions of the N 1s splitting peaks at 398.78 eV (NH_2—) and 400.24 eV (—NH—(C=S)—); after reacting with Cu^{2+} ions, the binding energies of the N 1s peaks were shifted to 399.75 and 400.99 eV, respectively, indicating that the electron density on the N atoms in AHS decreased. The N 1s spectra of original chalcopyrite indicated that there is no obvious of peaks could be observed. After the adsorption of AHS on the chalcopyrite surface, the N 1s bands at approximately 399.67 and 400.93 eV appeared on the chalcopyrite surface, which were very close to the values of the AHS-Cu^{2+} complex (399.75 and 400.99 eV, respectively). These findings indicated that the presence of Cu ions on the chalcopyrite surface changed the chemical circumstance of the N atoms in AHS, implying that AHS might interact with Cu ions to form complexes that form a layer on the surface of chalcopyrite.

The Fe 2p spectra of the original and AHS treated chalcopyrite are presented in Fig. 14. The peak at 711.59 eV could be assigned to iron (III)-O—OH, in agreement with the reported data [42,43]. This finding indicates that the chalcopyrite surface is oxidized, in agreement with the results of the S 2p spectra above. The other iron species detected in the investigation, in addition to iron oxides, are those bonded to sulphur at 707.69 eV, which correspond to iron species bonded with S; these peaks have been reported to be 708.2 eV (Fe(III)-S) [37], 707.4 eV (FeS) [36] and 707.5 eV (FeS_2) [44,45]. After the adsorption of AHS, there is no obvious shifting of the binding energy of the Fe 2p spectrum. The results

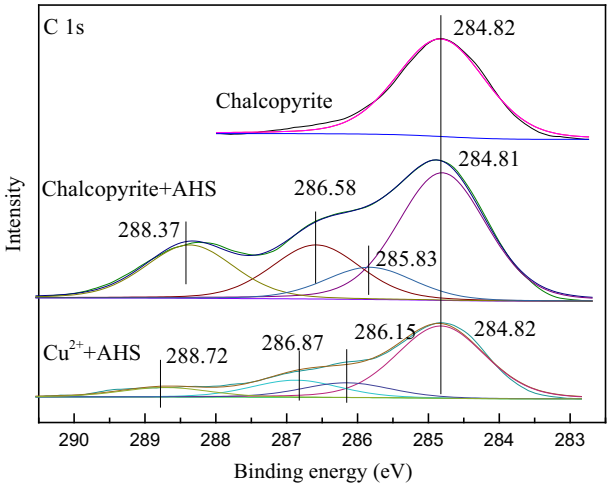

Fig. 12. C 1s spectra of the AHS + Cu^{2+}, chalcopyrite before and after treatment.

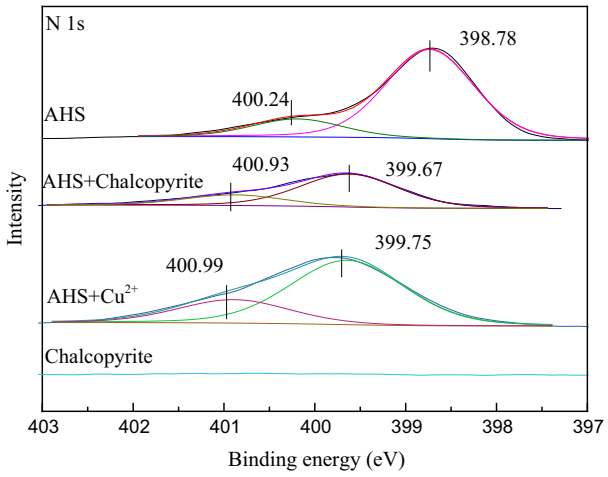

Fig. 13. N1s spectrum of AHS, AHS-Cu^{2+}, chalcopyrite before and after treatment.

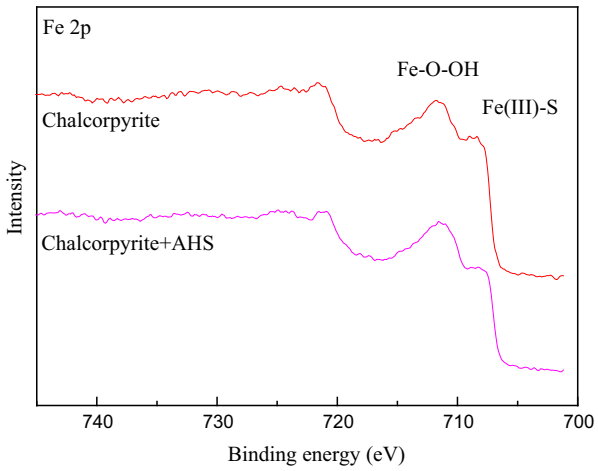

Fig. 14. Fe 2p XPS spectra of chalcopyrite before and after treatment.

indicate that the Fe 2p spectrum is not influenced by the adsorption of AHS. Therefore, a conclusion can be drawn that AHS had a weak effect on the chemical circumstance of the Fe atoms of chalcopyrite. In other words, the electron density of the Fe atoms changed insignificantly after the adsorption of AHS.

The O 1s spectra of chalcopyrite could be fitted by three components at 533.56, 532.03 and 530.91 eV, which are assigned to the adsorbed water, hydroxides and oxides (SO_4^{2-}) [46,47], respectively. These results imply that the oxidation products of chalcopyrite are expected at the mineral interface, in agreement with the S 2p and Fe 2p data of chalcopyrite mentioned above. The O 1s signals of depressant-treated chalcopyrite can be fitted into two components (Fig. 15). The peaks (532.68 eV and 531.35 eV) observed on depressant-treated chalcopyrite indicated that the C—O and C=O in AHS were found on chalcopyrite; this result is similar to that reported in the literatures [41,48]. Furthermore, the O 1s spectra of copper complex centered at around 531.42 and 532.62 eV, respectively, indicating that the electron of oxygen atoms in AHS molecular nearly the same as the oxygen atoms of AHS treated chalcopyrite and AHS (531.38 and 532.60 eV). Therefore, a conclusion could be drawn that the carboxyl group ($—COO^-$) of AHS is not the reaction site during the formation of metal complex.

In Fig. 16, the two peaks centred at approximately 932.30 and 952.17 eV represent Cu $2p_{3/2}$ and Cu $2p_{1/2}$ of chalcopyrite, respectively, in agreement with those reported in the literature [36,37].

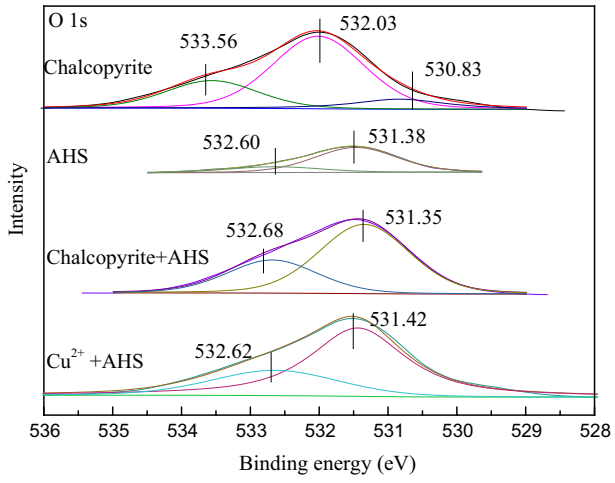

Fig. 15. O 1s XPS spectra of AHS, AHS-Cu^{2+}, chalcopyrite before and after treatment.

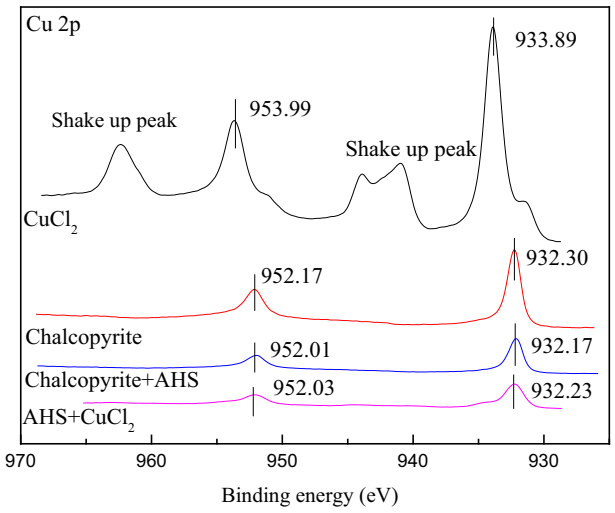

Fig. 16. The Cu 2p spectra of $CuCl_2$, AHS + Cu^{2+} complexes, chalcopyrite before and after treatment.

The Cu 2p binding energy located at 933.89 and 953.99 eV assign to Cu $2p_{3/2}$ and Cu $2p_{1/2}$ of copper dichloride. The copper peaks of the AHS-Cu^{2+} complexes were shifted to lower binding energies at 932.23 and 952.03 eV, which shifted to lower binding energy by 1.66 and 1.72 eV respectively, indicating that the electron density of copper ions changed. After AHS treatment, both Cu $2p_{3/2}$ and Cu $2p_{1/2}$ of chalcopyrite shifted to lower binding energies at approximately 932.17 and 952.01 eV, respectively; this result is very similar to the binding energy of the complexes. These downward shifts may be explained as an increase in the electronic density around cupper ions (Cu (I), Cu (II)) attributed to the electron donation of sulphur and nitrogen atoms present in the depressant molecule, thus providing further evidence of the possible chemical reaction between the depressant and chalcopyrite during the adsorption process.

3.6. The adsorption model

AHS is an anionic compound, and its main species mainly exist as anionic species ($(NH_2—NH—C(=S)—S—CH_2—COO)^-$) under alkaline conditions. As a result, after the adsorption of anionic species, the zeta potentials of chalcopyrite particles shifted to more negative values, inferring an increase of negative charges on the chalcopyrite surface. The results of FTIR inferred that AHS might be chemisorbed onto the chalcopyrite surface through its rearranged functional group $NH_2—N=C(—SH)—S—$ to form surface complexes on the chalcopyrite surface. XPS analysis further demonstrated that AHS reacts with Cu^{2+} and Cu^+ ions through its N and S atoms to form five-membered cheat rings. Based on the above findings, the predicted adsorption modes were postulated for the surface interaction between AHS and chalcopyrite (Fig. 17).

4. Conclusions

In this study, a novel depressant, acetic acid-[(hydrazinylthioxo methyl)thio]-sodium, was synthesized, and its flotation performances and adsorption mechanism to chalcopyrite were investigated via micro-flotation, kinetic flotation, and zeta potential measurements as well as FTIR and XPS measurements analyses. From the results of the investigation, the following conclusions can be drawn:

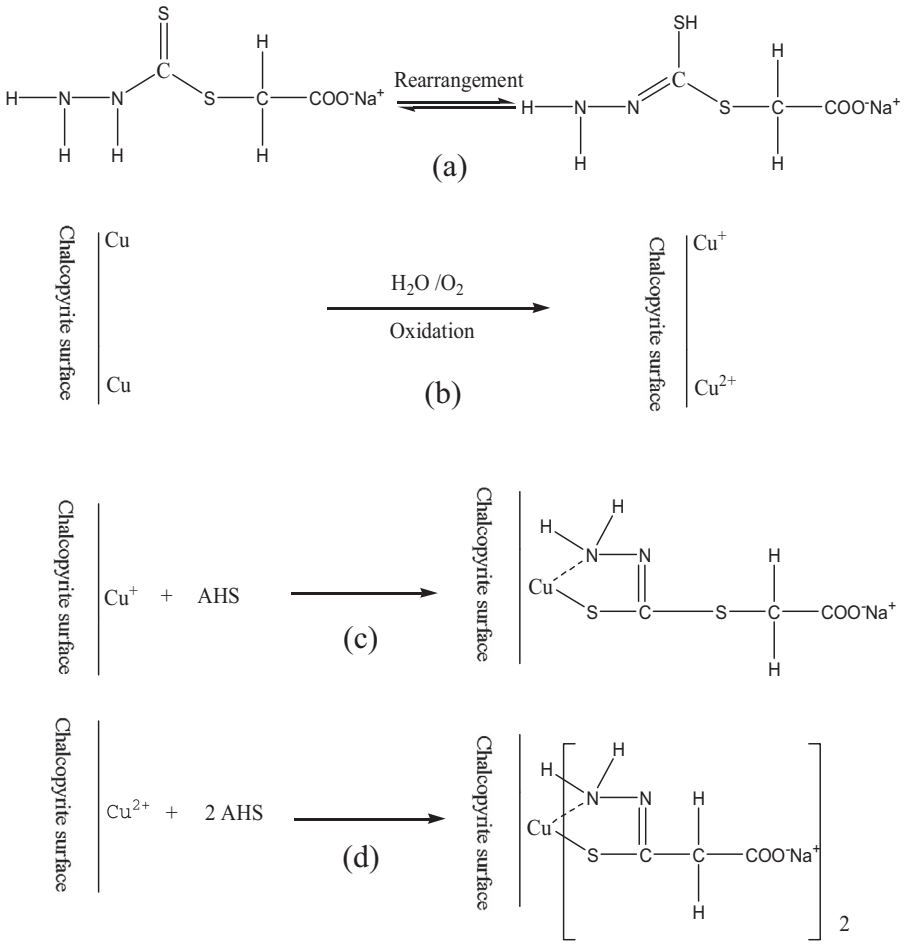

Fig. 17. The proposed adsorption models of AHS on the chalcopyrite surface (c and d).

(a) The results of the micro-flotation tests indicated that AHS exhibited superior depressing power to chalcopyrite and that selectivity against molybdenite and could effectively realize flotation separation of chalcopyrite under weak alkaline conditions.
(b) The results of batch flotation indicated that it is possible to adopt AHS as a selective depressant in copper-molybdenum separation, which has the advantages of a lower dosage and environmental compatibility. The molybdenite/chalcopyrite selectivity index in the presence of AHS is far better than that in the absence of AHS, indicating that AHS has a good selective depressing effect for chalcopyrite.
(c) For AHS with two polar groups, such as (NH_2—NH—C(=S)— and —COO^-, its functional group NH_2—NH—C(=S)—S—R rearranged into NH_2—N=C(—SH)—S—R, and then, the Cu ions bonded with S and N atoms to form five-membered chelate rings, while the S—H bonds were broken and released H ions into the aqueous solutions. The results of the FTIR, zeta potential and XPS measurements further confirmed that AHS chemisorbs onto the chalcopyrite surface.

Acknowledgements

The authors would like to acknowledge funding from the Innovation Driven Plan of Central South University (No. 2016zzts109); the National 111 Project (No. B14034); Sublimation Scholar's Distinguished Professor of Central South University; Collaborative Innovation Centre for Clean and Efficient Utilization of Strategic Metal Mineral Resources; Innovation Driven Plan of Central South University (No. 2015CX005); the National Science and Technology Support Project of China and Natural Science Foundation of China (No. 51374247). The authors also gratefully acknowledge the Yichun Luming Mining Co., Ltd. for sample collection and project discussion.

Appendix A. Supplementary material

Supplementary data associated with this article can be found, in the online version, at http://dx.doi.org/10.1016/j.seppur.2017.01.049.

References

[1] A. Ansari, M. Pawlik, Floatability of chalcopyrite and molybdenite in the presence of lignosulfonates, Part I. Adsorption studies, Miner. Eng. 20 (2007) 600–608.
[2] M.Y. Li, D.Z. Wei, Q. Liu, W.B. Liu, J.M. Zheng, H.J. Sun, Flotation separation of copper-molybdenum sulfides using chitosan as a selective depressant, Miner. Eng. 83 (2015) 217–222.
[3] M.S. Prasad, Reagents in the mineral industry recent trends and applications, Miner. Eng. 5 (1992) 279–294.
[4] Y.R. Jiang, L.H. Zhou, Y.L. Xue, J.G. Zhu, Separation of molybdenite from chalcopyrite using new depressant DPS, Min. Metall. Eng. 21 (2001) 33–36.
[5] W.Z. Yin, L.R. Zhang, F. Xie, Flotation of Xinhua molybdenite using sodium sulfide as modifier, Trans. Noferrous Met. Soc. China 20 (2010) 702–706.
[6] M. Poorkani, S. Banisi, Industrial use of nitrogen in flotation of molybdenite at the Sarcheshmeh copper complex, Miner. Eng. 18 (2005) 735–738.

[7] M.J. Pearse, An overview of the use of chemical reagents in mineral processing, Miner. Eng. 18 (2005) 139–149.
[8] J.H. Chen, L.H. Lan, X.J. Liao, Depression effect of pseudo glycolythiourea acid in flotation separation of copper-molybdenum, Trans. Noferrous Met. Soc. China. 23 (2013) 824–831.
[9] M.Y. Li, D.Z. Wei, W.G. Liu, S.L. Ca, G.Q. Liang, Selective depression effect in flotation separation of copper-molybdenum sulfides using 2,3-disulfanylbutanedioic acid, Trans. Nonferrous Met. Soc. China 25 (2015) 3126–3132.
[10] Y. Liu, Q. Liu, Flotation separation of carbonate from sulfide minerals, II: mechanisms of flotation depression of sulfide minerals by thioglycollic acid and citric acid, Miner. Eng. 17 (2004) 865–878.
[11] Z.G. Yin, W. Sun, Y.H. Hu, J.H. Zhai, Q.J. Guan, Evaluation of the replacement of NaCN with depressant mixtures in the separation of copper-molybdenum sulphide ore by flotation, Sep. Purif. Technol. 173 (2017) 9–16.
[12] Z.G. Yin, W. Sun, J.D. Liu, Y.H. Hu, Q.J. Guan, C.H. Zhang, H.H. Tang, C.P. Guan, Investigation into the flotation response of refractory molybdenum ore to depressant mixtures: a case study, Int. J. Mining. Sci. Technol. 26 (6) (2016) 1089–1094.
[13] J.M. Wie, D.W. Fuerstenau, The effect of dextrin on surface properties and the flotation of molybdenite, Int. J. Miner. Proces. 1 (1974) 17–32.
[14] A. Ansari, M. Pawlik, Floatability of chalcopyrite and molybdenite in the presence of ligosulfonates. Part I. Hallimond tube flotation, Miner. Eng. 20 (2007) 609–616.
[15] A. Beaussart, L. Parkinson, A. Mierczynsak-Vasilev, D.A. Beattie, Adsorption of modified dextrins on molybdenite: AFM imaging, contact angle, and flotation studies, J. Colloid. Interface Sci. 368 (2012) 608–615.
[16] M.A. Ali, M.T.H. Tarafdar, Metal complexes of sulphur and nitrogen-containing ligands: complexes of S-benzyldithiocarbazate and a Schiff base formed by its condensation with pyridine-2-carboxaldehyde, J. Inorg. Nucl. Chem. 39 (1977) 1785–1791.
[17] K.A. Crouse, K.B. Chew, M.T.H. Tarafder, A. Kasbollah, A.M. Ali, B.M. Yamin, H.K. Fun, Synthesis, characterization and bio-activity of S-2-picolydithiocarbazate (S2PDTC), some of its Sciff bases and their Ni(II) complexes and X-ray structure of S-2-picolyl-β-N-(2-acetylpyrrole)dithiocarbazate, Polyhedron 23 (2004) 161–168.
[18] E.N.M. Yusof, T.B.S.A. Ravoof, J. Jamsari, E.R.T. Tiekink, A. Veerakumarasivam, K. A. Crouse, M.I.M. Tahir, H. Ahmad, Synthesis, characterization and biological studies of S-4-methylbenzyl-β-N-(2-furylmethylene) dithiocarbazate (S4MFuH) its Zn^{2+}, Cu^{2+}, Cd^{2+} and Ni^{2+} complexes, Inorg. Chim. Acta 438 (2015) 85–93.
[19] R. Centore, R. Takjoo, A. Capobianco, A. Peluso, Ring to open-chain transformation induced by selective metal coordination in a new dithiocarbazate ligand, Inorg. Chim. Acta 404 (2013) 29–33.
[20] K. Tampouris, S. Coco, A. Yannopoulos, S. Koinis, Palladium(II) complexes with S-benzyl dithiocarbazate and S-benzyl-N-isopropylidenedithiocarbazate: synthesis, spectroscopic properties and X-ray crystal structures, Polyhedron 26 (2007) 4269–4275.
[21] E. Zangrando, M.S. Begum, M.C. Sheikh, R. Miyatake, M.M. Hossain, M.M. Alam, M.A. Hasnat, M.A. Halim, S. Ahmed, M.N. Rahman, Synthesis, characterization, density functional study and antimicrobial evaluation of a series of bischelated complexes with a dithiocarbazate Schiff base ligand, Arab. J. Chem. 10 (2) (2017) 172–184.
[22] P. Bera, C.H. Kim, S.II. Seok, Synthesis of nanocrystalline CdS from cadmium(II) complex of S-benzyl dithiocarbazate as a precursor, Solid State Sci. 12 (2010) 1741–1747.
[23] J. Pyun, K. Matyjaszewski, Synthesis of nanocomposite organic/inorganic hybrid materials using controlled/"living" radical polymerization, Chem. Mater. 13 (2001) 3436–3448.
[24] C.F. Wise, D. Liu, K.J. Mayer, P.M. Crossland, C.L. Hartley, W.R. McNamara, A nickel complex of a conjugated bis-dithiocarbazate Schiff base for the photocatalytic production of hydrogen, Dalton. Trans. 44 (2015) 14265–14271.
[25] P. Bera, C.H. Kim, S.II. Seok, Synthesis spectroscopic characterization and thermal behavior of cadmium(II) complexes of S-methyldithiocarbazate (SMDTC) and S-benzyldithiocarbazate (SBDTC) X-ray crystal structure of [Cd (SMDTC)3]·$2NO_3$, Plyhedron 27 (2008) 3433–3438.
[26] M.Q. Xu, Modified flotation rate constant and selectivity index, Miner. Eng. 11 (1998) 271–278.
[27] S.X. Song, X.W. Zhang, B.Q. Yang, A. Lopez-Mendoze, Flotation of molybdenite fines as hydrophobic agglomerates, Sep. Purif. Technol. 98 (2012) 451–455.
[28] S. Chander, On the natural floatability of molybdenite, Trans. AIME 252 (1972) 62–68.
[29] Y. Yu, Y.Y. Ge, X.L. Guo, W.B. Guo, The depression effect and mechanism of NSFC on dolomite in the flotation of phosphate ore, Sep. Purif. Technol. 161 (2016) 88–95.
[30] T.K. Mitchell, A.V. Nguyen, G.M. Evans, Heterocoagulation of chalcopyrite and pyrite minerals in flotation separation, Adv. Colloid. Interface. Sci. 114–115 (2005) 227–237.
[31] L. Reyes-Bozo, M. Escudey, E. Vyhmeister, et al., Adsorption of biosolids and their main components on chalcopyrite, molybdenite and pyrite: zeta potential and FTIR spectroscopy studies, Miner. Eng. 78 (2015) 128–135.
[32] S.H. Du, Z.F. Luo, Flotation technology of refractory low-grade molybdenum ore, Int. J. Mining. Sci. Technol. 23 (2013) 255–260.
[33] M.A. Ali, R. Bose, Metal complexes of Schiff bases formed by condensation of 2-methoxybenzaldehyde and 2-hydroxyenzaldehyde with S-benzyldithiocarazate, J. Inorg. Nucl. Chem. 39 (1977) 265–269.
[34] L.L. Sheng, J.Y. Wu, Y.P. Tian, Y.W. Tang, M.H. Jiang, H.K. Fun, S. Chantrapromma, Preparation, characterization, two-photo absorption and optimal limiting properties of a novel metal complex containing, Opt. Mater. 28 (2006) 897–903.
[35] Y. Yang, S. Harmer, M. Chen, Synchrotro X-ray photoelectron spectroscopic study of the chalcopyrite leached by moderate thermophiles and mesophiles, Miner. Eng. 69 (2014) 185–195.
[36] A. Ghahremaninezhad, D.G. Dixon, E. Asselin, Electrochemical and XPS analysis of chalcopyrite (CuFeS2) dissolution in sulfuric acid solution, Electrochim. Acta 87 (2013) 97–112.
[37] Y. Yang, S. Harmer, M. Chen, Synchrotro-based XPS and NEXAFS study of surface chemical species during electrochemical oxidation of chalcopyrite, Hydrometallurgy 156 (2015) 89–98.
[38] C. Klauber, A. Parker, W.V. Bronswijk, H. Watling, Sulphur speciation of leached chalcopyrite surfaces as determined by X-ray photoelectron spectroscopy, Int. J. Miner. Proces. 62 (2001) 65–94.
[39] A.N. Buckley, G.A. Hope, K.C. Lee, E.A. Petrovic, R. Woods, Adsorption of O-isopropyl-N-ethyl thionocarbamate on Cu sulfide ore minerals, Miner. Eng. 69 (2014) 120–132.
[40] R. Szargan, S. Karthe, XPS studies of xanthate adsorption on pyrite, Appl. Surf. Sci 55 (1992) 227–232.
[41] G. Farithorne, D. Fornasiero, J. Ralston, Formation of a copper-butyl ethoxycarbonyl thiourea complex, Anal. Chim. Acta 346 (1997) 237–248.
[42] S.L. Harmer, J.E. Thomas, D. Fornasiero, A.R. Gerson, The evolution of surface layers formed during chalcopyrite leaching, Geochim. Cosmochim. Ac. 70 (2006) 4392–4402.
[43] Y. Kalegowda, Y.L. Chan, D.H. Wei, S.L. Harmer, X-PEEM, XPS and TOF-SIMS characterization of xanthate induced chalcopyrite flotation: effect of pulp potential, Sur. Sci. 635 (2015) 70–77.
[44] S. Karthe, R. Szargan, E. Suoninen, Oxidation of pyrite surfaces: a photoelectron spectroscopic study, Appl. Surf. Sci. 72 (1993) 157–170.
[45] Å. Sandström, A. Shchukarev, J. Paul, XPS characterisation of chalcopyrite chemically and bio-leached at high and low redox potential, Miner. Eng. 18 (2005) 505–515.
[46] J.A. Mielczarski, J.M. Cases, M. Alnot, J.J. Ehrhardt, XPS characterization of chalcopyrite, tetrahedrite, and tennantite surface products after different conditioning. 1. Aqueous solution at pH 10, Langmuir 12 (1996) 2519–2530.
[47] M.J. Deng, D. Karpuzov, Q.X. Liu, Z.H. Xu, Cryo-XPS study of xanthate adsorption on pyrite, Sur. Interface Anal. 45 (2013) 805–810.
[48] X. Ma, Y. Hu, H. Zhong, S. Wang, G.Y. Liu, G. Zhao, A novel surfactant S-benzoyl-N,N-diethyldithiocarbamate synthesis and its flotation performance to galena, Appl. Surf. Sci. 365 (2016) 342–351.